Simulation-Based Assessment of Excessive Frequency Support Behavior of Electric Vehicles

Angela Popova, Soupayan Bose, Reinaldo Tonkoski
Chair of Electric Power Transmission and Distribution
Technical University of Munich
Munich, Germany
angela.popova, soupayan.bose, reinaldo.tonkoski@tum.de

Ulrike Schönlein, Barbara Weinzerl, Stefan Horn
System Operations — System Balance
TenneT TSO GmbH
Bayreuth, Germany
ulrike.schoenlein, barbara.weinzerl, stefan.horn@tennet.eu

***Abstract*—Aggregated electric vehicles (EVs) are promising geographically distributed providers of frequency containment reserve (FCR). However, uncertainty remains about EV participation volumes and controller parameterization. This study therefore assesses, from a large-scale system perspective, the conditions under which additional frequency-responsive EV behavior beyond dimensioned and procured FCR, may compromise frequency stability. A dynamic simulation framework is developed using a reduced grid model of the synchronous area of Continental Europe (CE). Standard frequency-quality metrics are used to assess how control parameters (droop, latency, and filtering) influence stability across three system mixes and two contingency sizes. Results show that instability is not inherently linked to EV penetration levels but arises from adverse combinations of control gain and aggregate latencies. The study proposes inertia-dependent, practical tuning guidelines for safe operation, favoring moderate droop and strict delay limits to ensure reliable participation of supplementary EV-based FCR in future operational frameworks.**

***Index Terms*—Frequency containment reserve (FCR), frequency stability, electric vehicles (EVs).**

I. Introduction

Electrification of the transportation sector is accelerating across Europe, with the number of electric vehicles (EVs) projected to grow rapidly over the next decades [1], [2]. At the same time, it has been challenging to maintain frequency quality in the synchronous area of Continental Europe (CE) [3]. Traditional frequency containment reserve (FCR) provided by large synchronous generators is becoming insufficient due to increasing shares of inverter-based renewable generation, motivating new distributed providers capable of fast, controllable response. Among emerging options, EVs offer a geographically distributed source for FCR. When aggregated through vehicle-to-grid (V2G) control, EV fleets can provide active power adjustments proportional to frequency deviations, emulating a droop response. Given the projected fleet sizes [2], aggregated EVs could supply a substantial portion of CE's total FCR requirement.

However, this potential introduces new technical and regulatory challenges: EV participation is inherently variable, subject to communication delays and influenced by local charging patterns and user behavior. Moreover, there is currently no harmonized European framework which mandates frequency-sensitive behavior for EVs or their charging infrastructure, only default droop gradient guidance [4]. This regulatory uncertainty makes it essential to quantify how large-scale EV-based FCR could impact frequency stability

While the literature is rich on EV fleet modeling for V2G, smart charging and distribution level impact [5]–[7], fewer studies address large-scale system frequency stability when EVs provide FCR. However, a recent study performed on an island grid suggest that long activation delays (7-10 s) can have a destabilizing effect on system frequency [8].

This study addresses several open questions through simulation-based analysis using a reduced CE transmission grid model aligned with ENTSO-E frequency-quality criteria [9]. Initially it is assessed whether an upper bound exists for the share of EV-based FCR beyond which destabilizing effects on system frequency emerge. It is further investigated which delay and gain thresholds can ensure stable FCR provision under three different levels of system inertia.

The results provide design guidelines, aiming to support the definition of requirements for EV participation in FCR frameworks and contribute to a secure integration of distributed flexibilities in low-inertia grids.

II. Design of the simulation-based framework

To evaluate the system level effects of EV-based FCR, a simulation framework is developed as illustrated in Fig. 1.

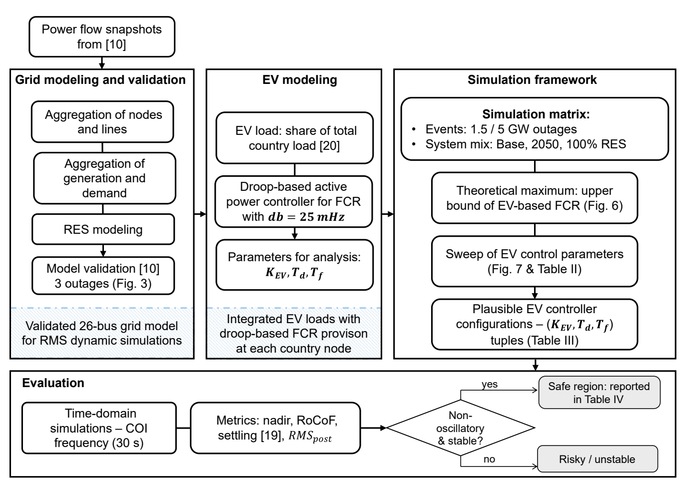

Fig. 1. Design of the simulation-based framework.

979-8-3315-8138-1

A. *Grid model and validation*

Frequency stability analysis requires a grid model suitable for RMS dynamic simulations. Therefore, the ENTSO-E Dynamic Model V2 [10] was obtained and implemented in DIgSILENT PowerFactory 2024. The model represents a credible 2027 CE grid model, developed for frequency and inter-area oscillation studies and validated against a real plant outage, ensuring realistic frequency dynamics. However, to represent and scale future scenarios with high RES penetration in a computationally efficient manner, a reduced 26-bus country-aggregated grid model was derived based on [10]. The process is visualized in Fig. 1. Firstly, all 380 kV and 220 kV transmission nodes within a country were aggregated to a geographic centroid-based equivalent of node coordinates from the model derived in [11]. Cross-border interconnectors were merged into equivalent tie-lines preserving impedance and circuit number [12]. Thermal and hydro power plants were clustered into country-level equivalent generators by summing the power outputs and using power-weighted averages for inertia constants (H). Country-level active and reactive demand was summed and assigned to each country bus. Wind, solar PV and grid-scale battery energy storage systems (BESS) were modeled as static generators with shares derived from [13] - [16]. Projections for BESS were distributed per country using population-based shares. Fig. 2 illustrates the resulting 26-bus model and a representative bus configuration.

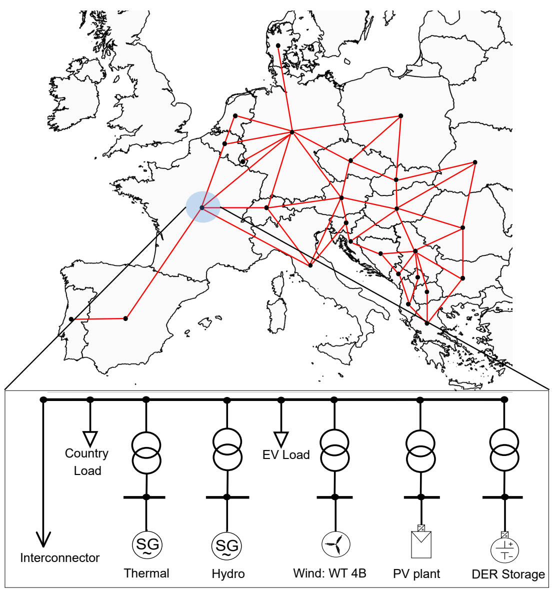

Fig. 2. 26-bus representation of the CE synchronous grid.

The 26-bus model was validated against [10] by three generator trips: 3 GW in Germany, 1 GW in Spain, and 1.5 GW in France. The COI frequencies in Fig. 3 show that the reduced model reproduces key dynamics with good fidelity. Minor discrepancies arise from structural differences (inclusion of Kosovo and exclusion of Turkey) and conventional power plant controller configurations. Synchronous generator controllers in the reduced model were adopted from [17], using SEXS and PSS2A for excitation with TGOV1 and HYDRO1 as governors. RES were modeled using WECC standard models: utility-scale PV plants and type 4B wind plants (RECC_D, REGC_B), with fast frequency response (FFR) capability for wind plants, and BESS (DER_A) [18], [19]. Frequency dependent load behavior was implemented as coefficient $k_{pf} = 1.5\%$ [9]. This combined modeling approach provides a computationally efficient yet dynamically credible simulation basis for evaluating frequency stability.

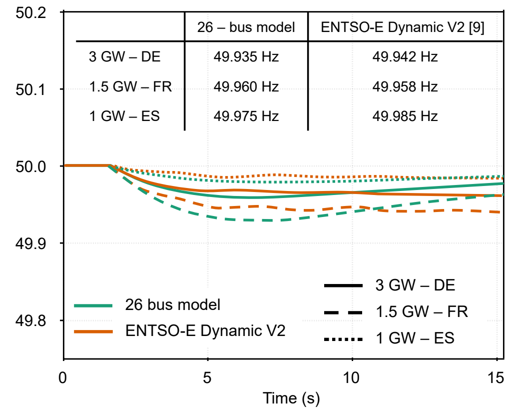

Fig. 3. Comparison of COI frequency: 26-bus model and [10].

B. *EV Modeling*

EVs are represented as additional, aggregated, controllable loads based on country-specific penetration. For country i:

$$P_{\mathrm{EV},i} = \alpha_i \cdot P_{\mathrm{Load},i}, \tag{1}$$

$P_{\mathrm{EV},i}$ is EV demand, $P_{\mathrm{Load},i}$ the base load, and α_i the EV share of country i [20]. The EV component is added at each bus while subtracting the same amount from the base load, preserving the operating point across EV-penetration scenarios.

EV participation in FCR is modeled as droop-based active power controller acting on local frequency measurements as shown in Fig. 4. The measured frequency f_{meas} is obtained via a phase-locked loop (PLL), filtered by a first-order low-pass filter (LPF) with time constant T_f, and subject to an aggregate measurement and actuation delay T_d. The adjustment dp_{ref} in p.u. is limited by the EV capacity ($p_{\min}$ and $p_{\max}$ in p.u.) and is computed based on the normalized frequency deviation $\Delta f = f_{meas} - f_n$ from nominal $f_{\mathrm{n}} = 50\,\mathrm{Hz}$:

$$dp_{\mathrm{ref}} = K_{\mathrm{EV}} \cdot \frac{\Delta f}{f_n} \;[\mathrm{p.u.}], \quad |\Delta f| \geq db,\; db = 25\,\mathrm{mHz}, \tag{2}$$

Here $K_{\mathrm{EV}} = 1/K$ is a dimensionless gain and K is the droop $(p.u.)$. The power control block applies dp_{ref} $(p.u.)$ to the measured aggregated EV demand P_{meas} (MW) to obtain the required EV power P_{fin}:

$$P_{\mathrm{fin}} = P_{\mathrm{meas}}\,(1 + dp_{\mathrm{ref}})\;[\mathrm{MW}]. \tag{3}$$

For an underfrequency event, $\Delta f < 0$ yields $dp_{\mathrm{ref}} < 0$, meaning charging is curtailed as P_{fin} reduces. By aggregating EV behavior at the transmission level, the model captures collective dynamic effects while remaining computationally efficient and suitable for system level frequency stability

979-8-3315-8138-1

studies [9], focusing on EV system-level interactions rather than device-level heterogeneity.

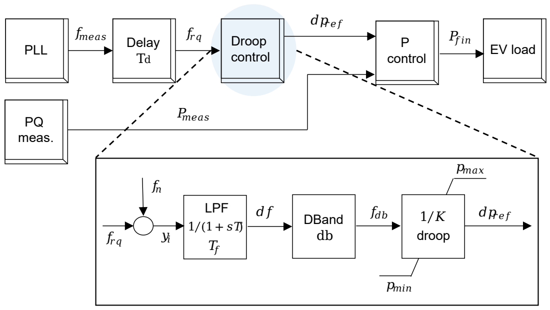

Fig. 4. Droop control of EV for FCR provision.

TABLE I
SIMULATION FRAMEWORK: EVENT SIZE AND SYSTEM MIX.

Dimension	Case	Definition
Event size	Large	5 GW step generation loss; larger than CE normative incident [9] - extreme condition.
	Small	1.5 GW step generation loss; smaller than CE normative incident [9] - plausible.
System mix	Base (2027)	Validated against [10] without wind and PV. $H_{\mathrm{sys}} = 5.02\,\mathrm{s}\ /\ 1759\,\mathrm{GW}\cdot\mathrm{s}$.
	2050	High penetration of wind 38% and PV 24%. $H_{\mathrm{sys}} = 4.85\,\mathrm{s}\ /\ 674\,\mathrm{GW}\cdot\mathrm{s}$.
	100% RES	Converter dominant case with wind 52% and PV 38%; 10 % hydro and 0 % thermal units. $H_{\mathrm{sys}} = 4.33\,\mathrm{s}\ /\ 167\,\mathrm{GW}\cdot\mathrm{s}$.

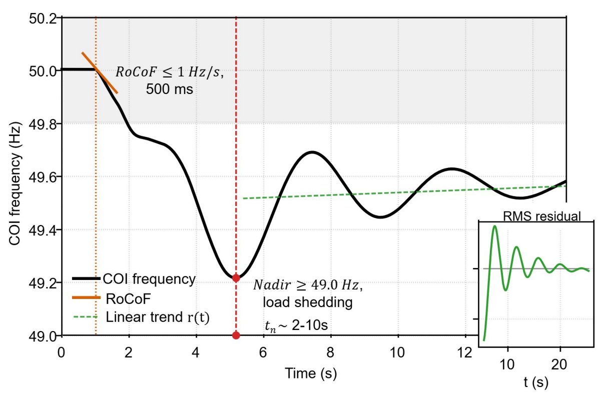

Fig. 5. Frequency quality evaluation metrics.

C. Simulations framework and evaluation metrics

The simulation framework in Fig. 1 was organized along two axes (Table I): event size and system mix. A theoretical upper bound on EV-based FCR was first assessed under full availability and favorable control settings. Subsequently, systematic variation of the EV FCR control parameters (K_{EV}, T_d and T_f) quantified their impact on frequency stability. In addition, four plausible configurations were evaluated specified by parameter tuples ($K_{EV},\ T_d,\ T_f$) derived from [21], [22].

Results are presented using time-domain COI frequency behavior and standard frequency-quality metrics according to [9] and illustrated in Fig. 5. To quantify post-nadir oscillations, a detrended RMS index is introduced. With $f(t)$ being COI frequency and t_{n} time of nadir, over a defined time window T_{w}, the analysis interval is defined as $[t_{\mathrm{n}},\ t_{\mathrm{n}} + T_{\mathrm{w}}]$. Within this window a linear trend $\hat{f}(t) = at + b$ is fitted using least-squares, and the residual is defined as $r(t) = f(t) - (at + b)$. The linear trend removes slower frequency recovery to settling frequency so that the metric captures only oscillation. The index is determined as:

$$\mathrm{RMS}_{\mathrm{post}} = \sqrt{\frac{1}{T_{\mathrm{w}}} \int_{t_0}^{t_1} r(t)^2\,\mathrm{d}t}\ [\mathrm{mHz}], \tag{4}$$

Higher values of RMS_{post} indicate stronger and/or more sustained post-nadir oscillations. In this study, RMS_{post} is assessed using a time window of $T_{\mathrm{w}} = 30\,\mathrm{s}$, matching the duration of the simulations. Values of $RMS_{post} \geq 30\,\mathrm{mHz}$ are considered risky for frequency stability (single post-nadir swing with amplitude $\geq 50\,\mathrm{mHz}$). This value is study-specific and not intended as a universal operational limit.

III. TECHNICAL LIMITATIONS OF EV-BASED FCR

Initially, it was investigated whether there is an upper bound for the share of EV-based FCR beyond which frequency stability deteriorates. This analysis assumes ideal control conditions with zero latency $T_d, T_f = 0\,\mathrm{s}$ and modest gain $K_{EV} = 3\%$ to isolate the intrinsic system effect of EV penetration. The EV share in total demand was gradually increased until degradation was detected in any of the standard frequency quality indicators. The 26-bus reduced model remained numerically stable for EV penetration of 100% of the total country load.

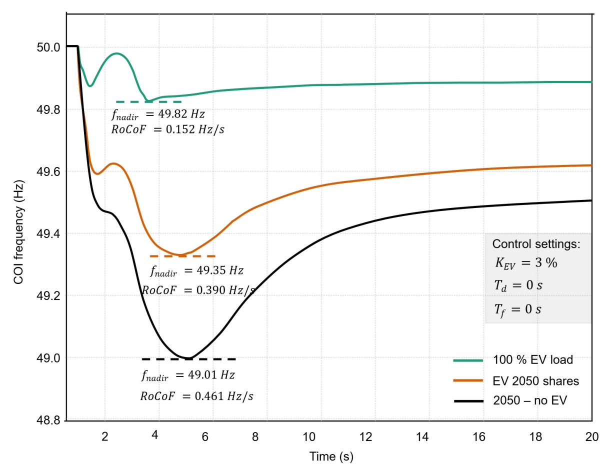

Fig. 6. Impact of EV penetration levels (large event).

As shown in Fig. 6 for system mix 2050, higher EV penetration under these assumptions improved the initial frequency containment without introducing post-nadir oscillations or instability and maintained all standard frequency-performance metrics within acceptable ranges. These results indicate that EV-based FCR participation, even at very high penetration levels and reduced system inertia, does not inherently threaten frequency stability, if latency is minimized and droops are moderate. The dominant limiting factor is thus the interaction between aggregate control delays and droop gain, quantified in the following sections.

979-8-3315-8138-1

TABLE II
SENSITIVITY OF f_{NADIR} AND ROCOF TO EV PARAMETERS.

Parameter	Setting	f_{nadir} (Hz) Base	2050	100% RES	RoCoF (Hz/s) Base	2050	100% RES
T_d [s]	0.5	49.82	49.65	49.22	0.140	0.398	0.362
	1.0	49.80	49.64	/	0.141	0.407	1.394
	2.0	49.78	49.61	/	0.141	0.414	3.780
T_f [s]	0.1	49.82	49.66	49.29	0.140	0.395	0.345
	0.2	49.82	49.66	49.27	0.141	0.401	0.352
	0.5	49.82	49.65	49.23	0.141	0.407	0.347
K_{EV} [%]	3	49.82	49.66	49.31	0.141	0.386	0.333
	5	49.83	49.70	49.45	0.138	0.376	0.294
	10	49.86	49.78	49.65	0.136	0.347	0.226

IV. IMPACT OF EV FCR CONTROL PARAMETERS

A systematic parameter study quantifies how three tuning variables of the EV droop controller: the aggregate measurement and actuation delay T_d, the LPF time constant T_f, and the droop gain K_{EV} affect system frequency stability for the three system mixes given in Table I. Each of the parameters is varied one at a time while the other two remain fixed at initial values ($T_d, T_f = 0\,\text{s}$, $K_{EV} = 3\%$). Fig. 7 and Table II summarize the sensitivity of the COI frequency to these parameters.

It can be observed that increasing the droop gain K_{EV} enhances initial frequency containment by amplifying EV response to frequency deviations (Fig. 7, top left). Larger T_f acts as additional delay, leading to slower reaction to changes in frequency and promoting oscillatory behavior. This effect is more pronounced in low-inertia systems such as 100% RES (Fig. 7, bottom left). Larger T_d forces the controller to act on outdated frequency information, leading to delayed corrections, longer settling times and in some cases frequency instability (e.g., 100% RES, $T_d \geq 0.5\,\text{s}$, Fig. 7, top right).

A sweep of parameter combinations was also performed to evaluate the joint impact of droop gain and delay parameters, aiming to identify practical tuning ranges and the limits of frequency stability. Representative results are shown as a heatmap in Fig. 7 for system mix 2050. The color coding of the heatmap denotes the nadir (f_n), i.e., deeper green indicates better nadir values. Additionally, the heatmap denotes time of nadir (t_n), settling time (t_s) and RMS_{post}. The sweep demonstrates that the total delay $T_\Sigma = T_d + T_f$ (considering T_f as additional delay) is the primary risk driver for frequency instability. As total delay T_Σ increases, the frequency oscillations after nadir increase significantly, reflected in higher RMS_{post} values. The most critical conditions arise when a large T_Σ is combined with a steep droop gain (e.g., 10%). In these cases, the controller reacts late yet forcefully, producing delayed overcorrection and sustained oscillations. The heatmap shows that in the 2050 mix, frequency instability is observed at $T_\Sigma = 2\,\text{s}$, and droop gain $K_{EV} = 10\%$. With the same delay but a more moderate droop gain of 5%, system frequency remains stable, however with pronounced oscillations ($RMS_{post} = 39\,\text{mHz}$).

A. Plausible EV controller configurations

To further assess a range of plausible EV controller configurations, four representative scenarios were defined:

TABLE III
METRICS BY SCENARIO: NADIR / t_N / t_S / RMS_{post} IN [Hz / s / mHz].

(a) Large contingency

Scenario	Base	2050	100% RES
B	49.86 / 0 / 9.03	49.78 / 5.80 / 10.58	49.65 / – / 11.49
RP	49.82 / 0 / 14.66	49.68 / 10.52 / 18.00	unstable
RN	49.80 / 0 / 17.88	49.61 / 12.61 / 39.28	non-convergent
W	49.79 / 0 / 54.19	unstable	non-convergent

(b) Small contingency

Scenario	Base	2050	100% RES
B	49.98 / 0 / 1.58	49.96 / 0 / 1.29	49.81 / 3.55 / 13.90
RP	49.97 / 0 / 2.05	49.88 / 0.01 / 11.17	unstable
RN	49.97 / 0 / 2.12	49.86 / 0.01 / 21.27	non-convergent
W	49.97 / 0 / 3.89	unstable	non-convergent

unstable = frequency does not settle after disturbance / exhibits sustained oscillations; *non-convergent* = RMS simulation fails numerically after large excursions and rapidly growing post-nadir oscillations (treated as outside the stable operating region).

- B (Best): $K_{EV} = 10\%$, $T_d = 0\,\text{s}$, $T_f = 0\,\text{s}$
- RP (Realistic +): $K_{EV} = 5\%$, $T_d = 1\,\text{s}$, $T_f = 0.05\,\text{s}$
- RN (Realistic -): $K_{EV} = 5\%$, $T_d = 2\,\text{s}$, $T_f = 0.2\,\text{s}$
- W (Worst): $K_{EV} = 10\%$, $T_d = 5\,\text{s}$, $T_f = 0.5\,\text{s}$

The evaluation metrics: frequency nadir, settling time and RMS_{post} are reported in Table III. In the Base system mix, all scenarios remain stable, although the Worst case displayed strong oscillations presented with larger $RMS_{post} = 54\,\text{mHz}$. This is driven by the combination of large T_Σ and high droop gain, which produces a late but relatively strong corrective action. In the 2050 system mix, these effects intensify across all metrics: nadirs are deeper, recovery is slower, and oscillations are more pronounced. The Worst case becomes unstable regardless of the event size. The 100% RES system mix exhibits the highest sensitivity. Frequency remains stable only for the Best case. For the Realistic-Negative and Worst configurations, the frequency trajectories show rapidly increasing post-nadir oscillations and large frequency excursions, after which the RMS simulation fails numerically. For the large contingency, the Best case does not recover into the $\pm 200\,\text{mHz}$ band.

Across all mixes, dominant destabilizing factors are large aggregate delays combined with high droop gain. Sensitivities intensify as system inertia reduces. Table IV provides practical design rules for droop and delay combinations which are independent of the contingency size and ensure system level frequency stability. For Base/2050-like mixes, $K_{EV} \leq 5\%$ with $T_\Sigma \leq 2\,\text{s}$ should be targeted, while for converter-dominant mixes, K_{EV} should be $\leq 3\%$ with $T_\Sigma \leq 0.5s$.

TABLE IV
STABILITY ENVELOPE ACROSS SYSTEM MIXES.

Mix	H [s]	Safe (K_{EV}, T_Σ)	Unstable
Base	5.02	$K_{EV} \leq 5\%,\ T_\Sigma \leq 3\,\text{s}$	K=10%, $T_\Sigma \geq 5$ s
2050	4.85	$K_{EV} \leq 5\%,\ T_\Sigma \leq 2\,\text{s}$	K=10%, $T_\Sigma \geq 3$ s
100% RES	4.33	$K_{EV} \leq 3\%,\ T_\Sigma \leq 0.5\,\text{s}$	K=5%, $T_\Sigma \geq 1$ s

V. CONCLUSION

This paper evaluates the system-level impact of EV-based FCR on frequency stability using a validated 26-bus model

979-8-3315-8138-1

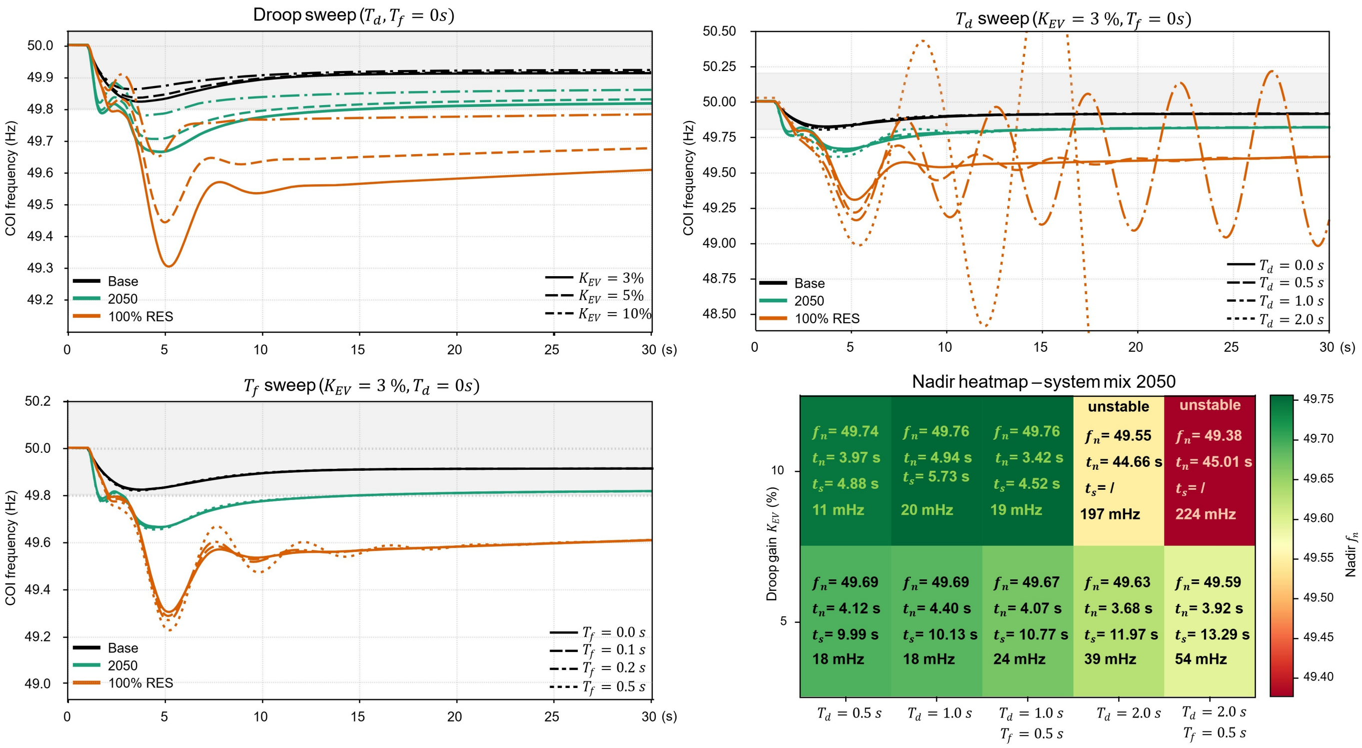

Fig. 7. EV parameter impacts across system mixes and delay–gain pairs (large contingency).

of the CE synchronous area and an aggregated EV droop controller. The results show that EV penetration is not the limiting factor: with negligible latency and moderate gain, frequency remains stable even at very high EV shares and reduced system inertia, and initial containment improves without inducing post-nadir oscillations. A parametric study across droop, measurement/actuation delay, and filtering for three inertia levels shows that stability is mainly governed by the gain-latency interaction with excessive delay-gain combinations causing oscillations and, in low-inertia mixes, instability. Representative design envelopes are derived for each system mix and are largely independent of the disturbance size. Under the adopted country-level aggregation and lumped EV response, these envelopes quantify the large-scale delay-gain impact, but do not represent local phenomena such as voltage dynamics, spatial heterogeneity in EV latency distribution, or local modes. Accordingly, the envelopes should be used as indicators of frequency stability for the CE synchronous area. Future work will extend the framework to spatially varying EV response and local frequency dynamics, and explore interactions with electrolyzers and large-scale heat pumps.

References

[1] International Energy Agency, *Global EV Outlook 2025*, Paris, May 2025.

[2] European Commission, "Sustainable and Smart Mobility Strategy - putting European transport on track for the future," Dec. 2020.

[3] ENTSO-E, "Annual Load-Frequency Control Report 2023," Sept. 2024.

[4] ENTSO-E SPD TF Inertia, "Investigation on default underfrequency support settings of new flexibilities in CE," Ver. 3.1, Apr. 2024.

[5] C. Ziras, J. Hu, S. You, H. W. Binder, "Modelling the aggregated dynamic response of electric vehicles," IEEE PES Innovative Smart Grid Technologies Conference Europe (ISGT-Europe), pg. 1-6, 2017.

[6] C. Peng, J. Zou, L. Lian, "Dispatching strategies of electric vehicles participating in frequency regulation on power grid: A review," Renewable and Sustainable Energy Reviews 68, pg. 147-152, 2017.

[7] H. R. Galiveeti, A. K. Goswami, N. B. Dev Choudhury, "Impact of plug-in electric vehicles and distributed generation on reliability of distribution systems," Engineering Science and Technology, an International Journal 21, pg. 50-59, 2018.

[8] A. Zecchino, M. Marinelli, and P. Andersen, "Large-scale frequency control via V2G: The Bornholm case," *Electr. Power Syst. Res.*, vol. 170, pp. 25–34, 2019.

[9] ENTSO-E RG CE, "Frequency stability evaluation criteria for the synchronous area of CE," 2016.

[10] ENTSO-E SG SPD, "Dynamic model of Continental Europe V2 - Public Report," June 4, 2024.

[11] Hewes, D., Altschaeffl, S., Boiarchuk, I. and Witzmann, R., "Development of a dynamic model of the European transmission system using publicly available data," ENERGYCON 2016.

[12] PyPSA Developers, "Network Clustering," *PyPSA Documentation*, v0.25.0, 2024.

[13] TRACER Project. *Energy Projections for 2030/2050 in Target Regions*.

[14] WindEurope. *Wind Energy in Europe: 2024 Statistics and Outlook*.

[15] Agora Energiewende. *Powering the Future of the Western Balkans with Renewables*. 2022.

[16] ENTSO-E/ENTSO-G (TYNDP), "Opportunities for a more efficient European power system by 2050," Apr. 9, 2025.

[17] ENTSO-E SG SPD, "Documentation on controller tests in test grid configurations," Nov. 26, 2013.

[18] WECC Renewable Energy Modeling Task Force, "WECC wind power plant dynamic modeling guide," Version 2, 2014.

[19] P. Pourbeik and D. Ramasubramanian, *Model user guide for generic renewable energy system models*, EPRI Report 3002027129, Oct. 2023.

[20] P. Kasten, J. Bracker, M. Haller, and J. Purwanto, *Assessing Electrification of Road Transport Passenger Vehicles and Implications for the EU Energy System*, Öko-Institut e.V., Sept. 2016.

[21] Aalborg Universitet. *Transient Stability Analysis of Droop-Controlled Grid-Connected Converters With Inertia Emulating Low-Pass Filters*. IEEE Energy Conversion Congress and Exposition (ECCE), 2019.

[22] *Delay-Dependent Stability Analysis of Load Frequency Control for Power System With EV Aggregator*. Frontiers in Energy Research, 2021.

979-8-3315-8138-1